OPTICAL FIBER STRAIN MEASUREMENTS AND NUMERICAL MODELING OF LOAD TESTS ON GROUTED ANCHORS

Jef Smet[1], Noël Huybrechts[1,2], Gust Van Lysebetten[2], Jan Verstraelen[3], and Stijn François[1]

[1]KU Leuven, Dept. of Civil Engineering, Kasteelpark Arenberg 40, B-3001 Leuven, Belgium.
Corresponding author: stijn.francois@kuleuven.be
[2]Belgian Building Research Institute (BBRI), Geotechnical Division, Avenue P. Holoffe 21, B-1342 Limelette, Belgium
[3]Smet Group, Kastelsedijk 64, B-2480 Dessel, Belgium

ABSTRACT

This paper reports on the behavior of a grouted anchor instrumented with a fiber optic strain sensor in the grout body along the entire anchor length. During load tests up to the estimated pull-out capacity, the strain measurements indicate that a delamination occurs in the tendon bond length between the steel tendons and the grout body. The upper delaminated part of the grout body is under compression, whereas the lower bonded part of the grout body is under tension. This delamination gradually progresses as the anchor load increases. Furthermore, a significant part of the load is transferred from the anchor to the soil in the tendon free length. The anchor behavior is further modeled with a one-dimensional finite element model that includes the steel tendons and the grout body, where an interface damage model is used to account for possible delamination of the interface. The numerical model confirms that the observed compressive and tensile strains in the grout can be related to a delamination of the steel strands in the tendon bond length. The experiment and numerical modeling demonstrate how optical fiber measurements in the grout body can be used, in operational conditions, to assess the anchor behavior, the mobilization of the soil resistance, and the estimation of the remaining anchor capacity.

INTRODUCTION

A grouted anchor is a foundation element that transfers tensile forces to the ground, commonly applied in the construction of retaining walls, to prevent uplift of foundation slabs, or for slope stabilization. Grouted anchors consist of steel strands installed in grout filled boreholes, where the strands and the grout are connected in the lower part of the anchor, referred to as the bond length. In order to increase the anchor pull-out capacity, gravity or pressure grouted anchors can be post-grouted, applying successive grout injections to enlarge the grout body and increase the soil stresses around the anchor.

The effect of the grout pressure on the anchor pull-out capacity is often estimated using cylindrical cavity expansion theory, where the radial soil stress is derived from plasticity models (Yu and Houlsby 1991; Mecsi 1997). However, such a theoretical approach commonly leads to an underestimation of the anchor pull-out capacity. In practice, the anchor pull-out capacity strongly depends on local soil conditions and installation factors such as the drilling technique, the grout pressure, and the (post-)grouting procedure. The influence between these installation factors and the resulting anchor capacity is not yet fully understood. Current anchor design is therefore based on

empirical correlations, taking into account various influence factors by means of correction factors, and supported by in situ performance and proof tests, as described in (inter)national standards and guidelines, e.g. NBN EN ISO 22477-5 (International Organization for Standardization 2018), NBN EN 1537 (Bureau for Standardisation (NBN) 2013), and NBN EN 1997-1/A1 (Bureau for Standardisation (NBN) 2014). Still, a large discrepancy is commonly observed between the design load and the actual anchor capacity. A realistic prediction of the anchor capacity therefore requires a thorough understanding of the mechanical behavior of the anchor.

In addition to this complex relation between various installation factors and the anchor pull-out capacity, a large statistical variability of the capacity is commonly observed on a particular construction site, even though the soil conditions and the installation procedure are very similar. The long term health monitoring of grouted anchors under operational conditions would allow to gain insight in the actual stress state in the grout and the tendons, and to estimate the remaining anchor capacity. Such an approach to monitoring of grouted anchors is the use of optical fiber technology, which nowadays allows for the accurate measurement of strains in geotechnical applications (Huang et al. 2013; Zeni et al. 2015). For grouted anchors, multiple research campaigns with optical fiber measurements (Huybrechts et al. 2017; Huybrechts et al. 2016; Štefaňák et al. 2017) have been performed. In these applications, an optical fiber has either been embedded within (Huang et al. 2013; Zeni et al. 2015) or glued on (Štefaňák et al. 2017; Gächter et al. 2018) the anchor tendon. A drawback of strain measurements of the anchor tendon is that embedding or gluing optical fibers on the strands is laborious and complicated. Furthermore, the fragile optical fiber may easily be pinched between the strands and break upon loading. As a result, the use of optical fibers in ground anchors (especially with strands) in engineering practice remains very limited, which is a pity because of its potential for long term health monitoring. Therefore, this paper presents and investigates a novel approach of measuring the strains in the grout body rather than on the steel tendons. A robust and cost-effective installation procedure has been developed, which is less laborious than gluing or embedding fibers on the anchor strands. The goal of this paper is to interpret the results of optical fiber strain measurements in the grout body and explore how these measurements can be used to assess the condition of the grouted anchor. Therefore, a construction site on the Health Sciences Campus of KU Leuven has been selected, on which a test anchor has been installed. Optical fibers have been embedded in the grout body, which allowed to measure the strains in the grout during the investigation tests up to the the estimated anchor pull-out capacity.

This paper is organized as follows: first, the relevant geotechnical parameters of the site are described and the installation of the anchor and the optical fiber is discussed. Next, the results of the load test are processed and the mechanical behavior of the grouted anchor is characterized. Furthermore, observations made during the anchor excavation are briefly discussed. A one-dimensional (1D) finite element (FE) model is finally set up and the numerical results are used to further interpret the test results.

SITE DESCRIPTION

On the construction site at the Health Sciences campus of KU Leuven, an underground parking lot has been constructed. The walls of the underground parking consist of secant piles, stabilized using grouted anchors. Apart from classical suitability and acceptance tests on the grouted anchors of the secant pile wall, an investigation test has been performed on a vertical test anchor, installed on the site prior to excavation.

The construction site is characterized by a relatively homogeneous sand layer crossing the

tertiary layers referred to as the Formation of Sint-Huibrechts-Hern. The soil in this formation has a varying color from brown-gray to brown-yellow and consists of fine sand particles with an admixture of clay and sporadic concentrations of iron oxide. The corresponding geotechnical parameters have been derived from cone penetration tests in the direct vicinity of the test anchor (figure 1), as well as oedometer and triaxial tests on soil samples from the same geological formation. The soil strength is characterized by a relatively high internal friction angle $\phi = 32.5°$ and cohesion $c = 8.5$ kPa, indicating that a relatively high anchor capacity can be expected.

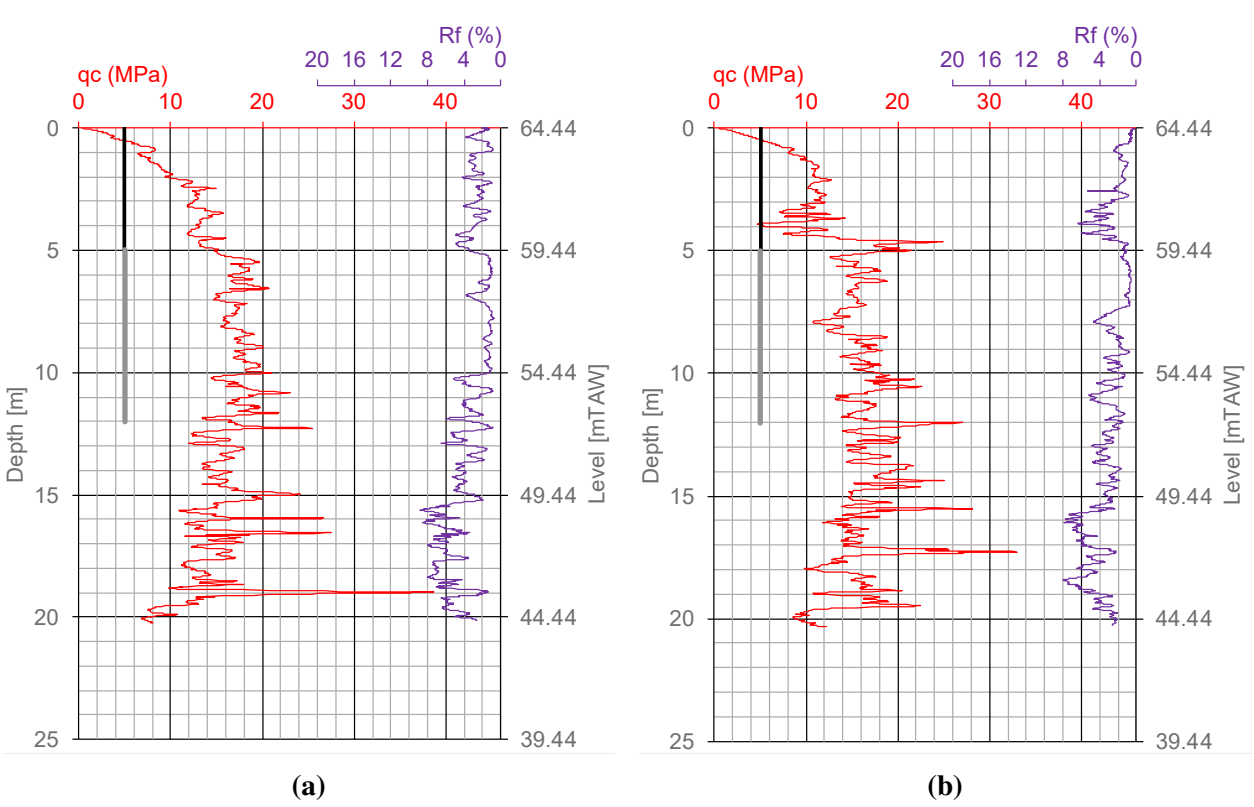

Fig. 1. Cone tip resistance q_c and friction ratio R_f from two CPT tests near the test anchor. The depth of the grouted anchor is also indicated.

INSTALLATION OF THE GROUTED ANCHOR

The test anchor consists of 9 steel strands of ST1660/1860 steel with a cross section of 150 mm^2 per strand (figure 2a). The anchor is grouted in a vertical borehole with a total anchor length of 15 m, consisting of 5 m tendon free length and 7 m tendon bond length. As the test anchor had a temporary and experimental purpose, no corrosion protection has been provided. In the tendon free length, the strands are surrounded by a plastic tube to prevent a rigid connection between steel and grout. Along each bundle of strands, 3 grout injection tubes are present (figure 2a). The grout injection tubes are used to perform high pressure post-grouting through 4 holes with a spacing of 1 m. 2 tubes are actually used during post-grouting, whereas the third tube is used as a spare.

The test anchor is equipped with an optical fiber to measure the strains along the grout body, based on the Brillouin optical fiber domain analysis (BOFDA) measurement technique (Hong et al.

2017). The BOFDA technique provides a distributed strain measurement, based on the fact that light is backscattered as the optical fiber deforms (Boyd 2003). Brillouin-based techniques are commonly applied in structural health monitoring of civil engineering structures, since they allow to measure strains globally with a fine spatial resolution and accuracy (Barrias et al. 2016). For the present application, the strains in the test anchor have been measured using a downward and upward optical fiber with an accuracy < 5 microstrain, averaged along the height of the anchor at a spatial resolution of 0.20 ± 0.05 m in the free length and 0.40 ± 0.05m in the bond length, so that local strain variations along the anchor are smoothed out.

The test anchor is bored with single drilling rods, so that the boring fluid returns through the annular space between the casing and the borehole. The drill bit, which remains in the ground after the installation of the anchor, has a diameter of 175 mm whereas the outer diameter of the casing is 133 mm.

In a first step, the drilling machine is positioned at the drilling location with the rig raised in a vertical position. The drilling rods are equipped with the drill bit (figure 2b) and driven into the ground using water as a drilling fluid (figure 2c). Once the final depth is reached, the borehole is flushed with water to remove loosened soil particles (figure 2d). Next, grout with a water/cement ratio of 0.5 is pumped through the drilling rods into the borehole. This allows the borehole to fill in a gravitational way (figure 2e). Once the borehole is completely filled, the drilling rods are disconnected from the drilling machine. A funnel is placed on top of the drilling rods to facilitate the lowering of the anchor strands in the borehole (figure 2f). At this stage, the optical fiber is installed (figure 2g). The optical fiber has been glued on a glass fiber-reinforced plastic carrier tube, which is gradually attached to the bundle of steel strands during lowering. This fiber-carrier system has been developed to provide a compromise between protection of the optic fiber and the reliability and accuracy of the deformation measurements. After the installation of the anchor strands and the optical fiber, all drilling rods are removed while additional grout is injected under gravitational pressure.

The installation of the grouted anchor is finalized with two post-grouting stages, where grout is injected under high pressure in the sleeved injection tubes, 4 and 12 hours after the installation of the anchor. This post-grouting increases the stresses in the soil surrounding the borehole which had loosened during to the drilling process. In addition, the post-grouting contributes to the roughness of the grout-soil interface. The increase of soil stresses and interface roughness significantly improves the ultimate capacity of the grouted anchor.

LOAD TEST

The test anchor was subjected to a load test 24 days after its installation. During the load test, a reaction frame has been positioned over the grouted anchor which allows to apply a tensile load by means of a hydraulic jack. The pressure in the hydraulic jack was maintained by a hydraulic pump within an accuracy of 1 bar. The axial displacement of the anchor head has been measured with respect to a reference system above the hydraulic jack and read out with a digital unit with an accuracy of 0.01 mm.

The test was executed in accordance with the corresponding norms, NBN EN ISO 22477-5 (International Organization for Standardization 2018) and NBN EN 1537 (Bureau for Standardisation (NBN) 2013), employing a maintained tension test (test method 3). The procedure prescribes a stepwise increase of the tensile force applied to the anchor head up to the proof load P_p. The proof load P_p should be smaller than 90 % of the yield strength of the steel strands. For the test anchor

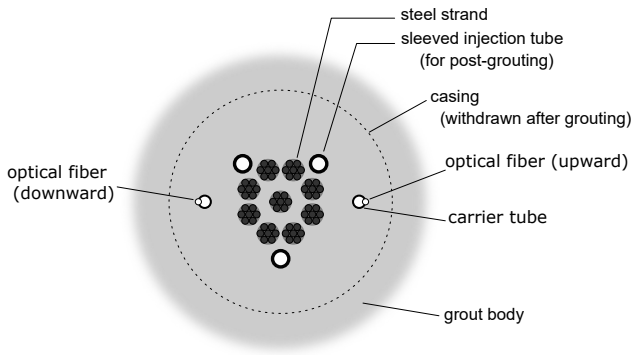

(a)

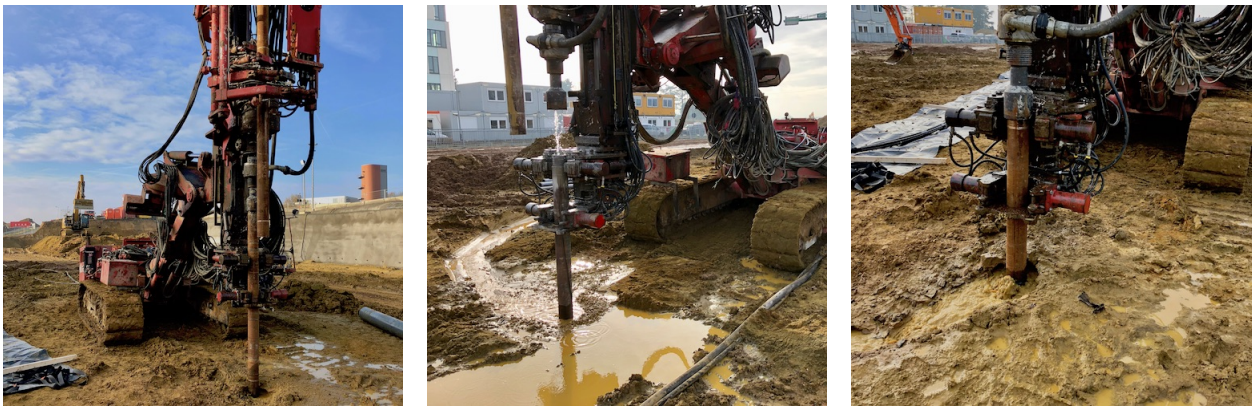

(b) **(c)** **(d)**

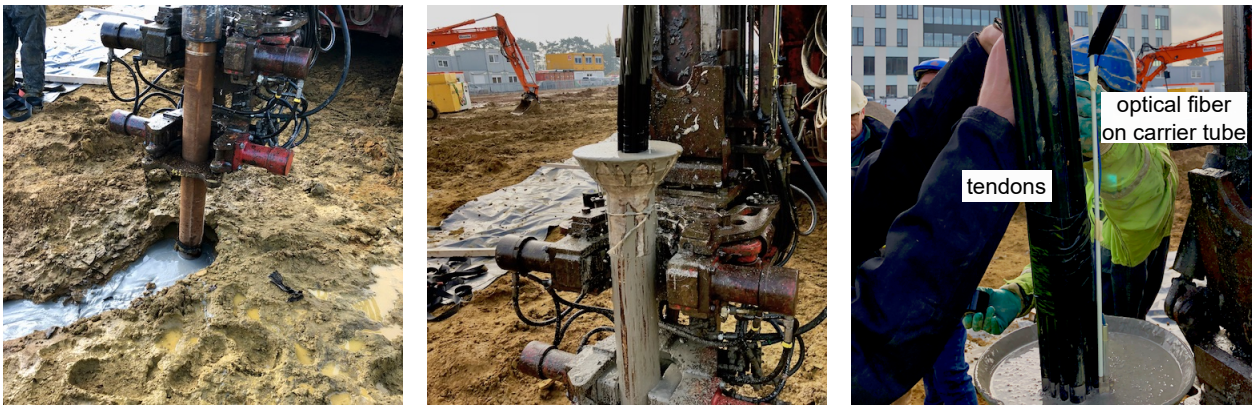

(e) **(f)** **(g)**

Fig. 2. Overview of the drilling process, including (a) cross-section of the grout anchor, (b) boring of the drilling rods into the ground, (c) installation of a second drill element with return boring liquid flowing out of the borehole, (d) flushing with water as the final depth is reached, (e) injection of grout until it flows out of the borehole, (f) decoupling of the drilling table from the rods for the installation of the anchor strands, and (g) installation of the optical fiber together with the steel strands.

with 9 strands of 150 mm^2 and a yield stress of 1660 MPa, the design yield force equals 2241 kN. As a result, the maximum test load was fixed to $P_\mathrm{p} = 2000$ kN, corresponding to the estimated anchor pull-out capacity based on experimental design curves for grouted anchors in sandy soils in Belgium (Huybrechts et al. 2008).

At the beginning of the test, a reference load smaller than 10% of the proof load P_p, is applied and the displacement is set to zero. Next, the load is increased with load steps of 250 kN. Each load step is maintained for 60 minutes, unless the creep rate α, defined as:

$$\alpha = \frac{s(t_2) - s(t_1)}{\log(t_2 - t_1)} \tag{1}$$

where $s(t_1)$ and $s(t_2)$ are the anchor head displacement at times t_1 and t_2, respectively, is lower than 1 mm. In that case, the duration of the load step is reduced to 30 minutes. During the load test, the creep rate limit of 1 mm was never reached, so that all load steps lasted 30 minutes. The unloading took place in 4 steps: 1500 kN, 1000 kN, 500 kN and 100 kN. The first 3 unloading steps were applied for 2 minutes, the last step for 5 minutes.

The load test has been performed up to the proof load of 2000 kN, indicating that the maximum tensile capacity of the grouted anchor was not reached and that the soil strength was not fully mobilized. The force-displacement curve is shown on figure 3, where the maximum anchor head displacement equals 79 mm.

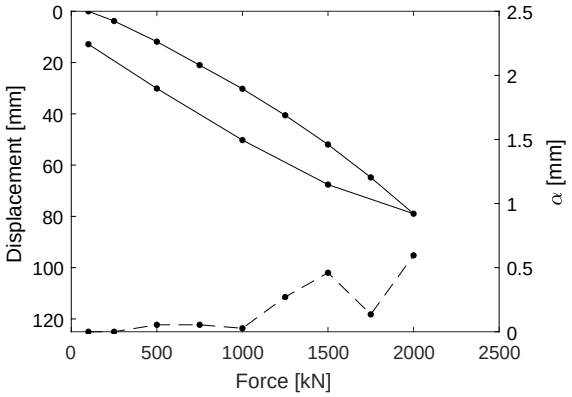

Fig. 3. Displacement (solid line) and creep rate (dashed line) of the anchor head as a function of the axial force during the load test.

The axial deformation of the grout body has been measured by means of the optical fibers during all load steps. The measured axial strain $\epsilon(z)$ in the grout along the anchor is plotted for each load step in figure 4a, where a tension positive convention is employed.

In general, it is expected that the grout body is overall in tension in the tendon bond length due to the transmission of the tensile force in the steel strands to the surrounding soil. However, figure 4a shows the counterintuitive result that some parts of the grout body are in compression while other parts are in tension. Correspondingly, four zones are distinguished as indicated on figure 4a, as discussed next. A small tensile strain is observed just below ground level at depths up to 1.5 m that is attributed to the stress state in the soil near the free surface. It is expected that these tensile strains in the tendon free length do not affect the global anchor behavior and are therefore not considered in the following.

Zone 1 is located in the tendon free length of the grouted anchor, where a plastic tube prevents the transmission of forces between the steel strands and the grout body. The axial strain is negative in this zone, i.e. the grout body is under compression. The absolute values of the deformation are small and increase with depth. This increase in axial strain denotes a limited transmission of shear forces between the grout column and the surrounding soil.

Zone 2, referred to as the influence zone, is located in the tendon free length at depths between 4 m and 5 m, just above the proximal end of the tendon bond length (i.e. the start of the tendon bond length). This zone is characterized by a strong increase in compressive axial strains. The grout body just above the tendon bond length is under compression. The large difference in axial strain between the top and bottom of zone 2 indicates the presence of shear forces between grout and soil. This is attributed to the fact that the grout body at the proximal end of the tendon bond length is broken and is being pushed upwards by the lower part of the anchor. This further results in compressive strains and stresses in the tendon free length.

Zone 3 is referred to as a transition zone, located in the upper part of the tendon bond length. A transition from compressive strains on the top of the zone towards tensile strains at the bottom of the zone are observed. The size of zone 3 depends on the magnitude of the applied tensile load: as the axial force increases towards 2000 kN, zone 3 extends downwards. Initially, there is a rigid connection between grout and steel in this zone so that it is expected that the grout and the steel strands have the same deformation. As the load is increased, compressive strains are observed in the grout body, which can no longer correspond to the (tensile) strain in the steel strands. This is attributed to a delamination between grout and steel, i.e. the grout body detaches from the tendons near the proximal end of the tendon bond length. This results in different deformation behavior of the steel and the grout.

Zone 4 represents the part of the grout body that has not delaminated from the steel strands and that pushes the broken grout upwards, inducing the negative (compressive) strains in zones 2 and 3. Below zone 4, at a depth of about 11.8 m, a peak in the tensile strain is observed at the load levels of 1750 kN and 2000 kN. This peak is attributed to the fact that the bottom part of 0.2 m of the grout body breaks at the end of the tendon bond length, resulting in a large extension of the glass fiber over the resulting crack.

The optical fiber measurements (figure 4a) provide the axial strain ϵ along the grout body at each load step. In order to subsequently estimate the axial force $F(z)$ from the measured strains, Fellenius' method (Fellenius 2001) is employed. Fellenius' method has originally been developed for interpreting static axial compressive tests on foundation piles with a composite section of grout/concrete and steel. The method is based on the assumption that the stress-strain behavior of the pile can be approximated by a second order polynomial. The method converges towards the strain dependent tangent modulus as the shaft resistance is being fully mobilized along the pile. Fellenius' method starts by plotting the ratio $\Delta F/\Delta\epsilon$ of the applied force increment ΔF and the measured strain increment $\Delta\epsilon$ as a function of the measured strain at all depths. This is done separately for zones 1, 2, and 4 (figure 5). The tangential stiffness is determined as the asymptotic value for large strains. In zone 1, the strains remain small and no clear limit value is reached. In zone 2, the tangential stiffness is estimated as $(EA)_{\text{grout}} = 270000\,\text{kN}$ and is attributed to the grout stiffness in compression. In zone 4, Fellenius method converges to a stiffness $(EA)_{\text{strands}} = 256500\,\text{kN}$ of the bundle of steel strands.

Subsequently, the estimated tangential stiffness values are used to compute the axial force of the anchor from the measured strains, as plotted in figure 4b. In zone 1, the tangential stiffness of

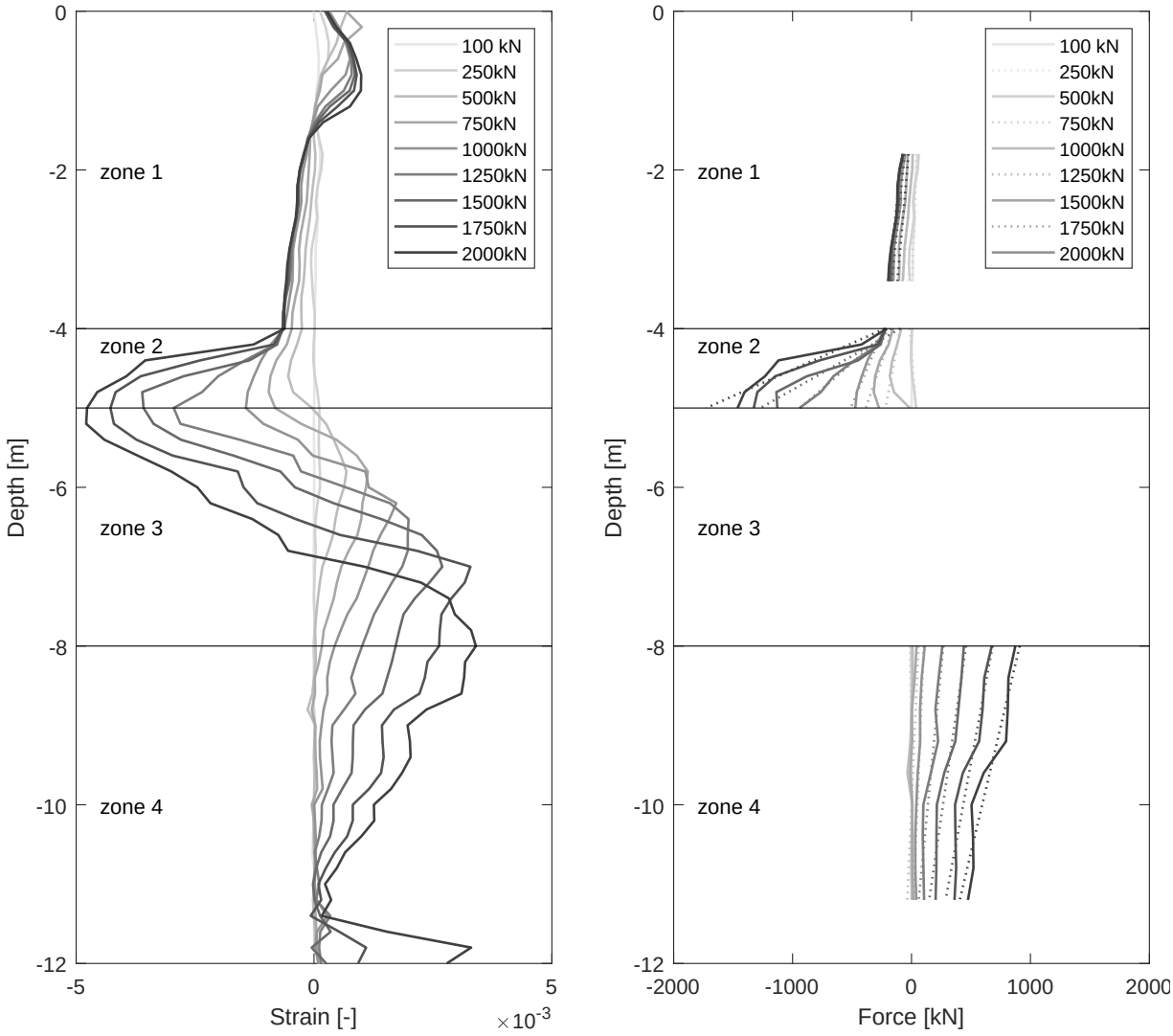

(a) $\epsilon(z)$ **(b)** $F(z)$

Fig. 4. (a) Axial deformation as a function of anchor head load during the load test, and (b) resulting estimate of the axial force in zones 1, 2, and 4 as determined with Fellenius' method. The average slope of the $F(z)$-curve is indicated with dashed lines.

zone 2 has been used to compute the axial force since no clear asymptote can be distinguished in figure 5a.

The estimated force $F(z)$, obtained with Fellenius' method is further used to compute the shear force $q(z)$ along the anchor body from the equilibrium of the grouted anchor as:

$$q(z) = -\frac{dF}{dz} \tag{2}$$

The shear force q is computed from the average slope of the force distribution for zones 1, 2, and 4 in figure 4b and plotted as a function of the anchor head displacement in figure 6. The resulting plots show an almost linear behavior, indicating that only a limited amount of the soil strength on

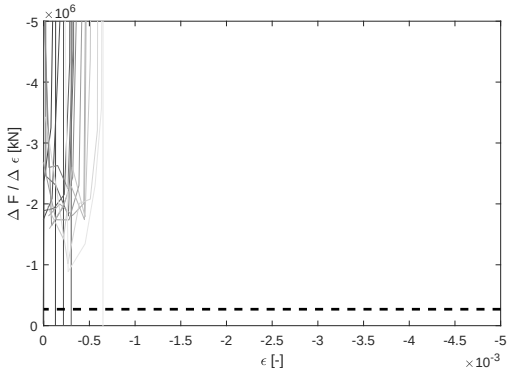

(a) Zone 1 - Depths from 1.6 m (light grey) to 3.8 m (dark grey).

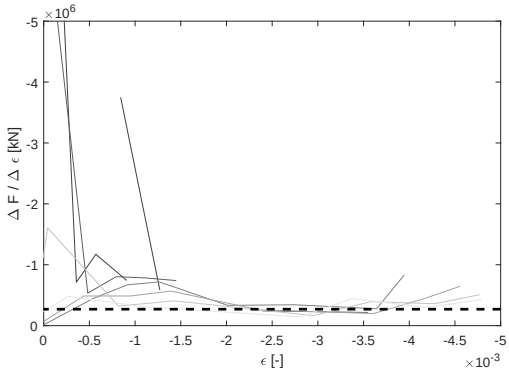

(b) Zone 2 - Depths from 4.2 m (light grey) to 5.2 m (dark grey).

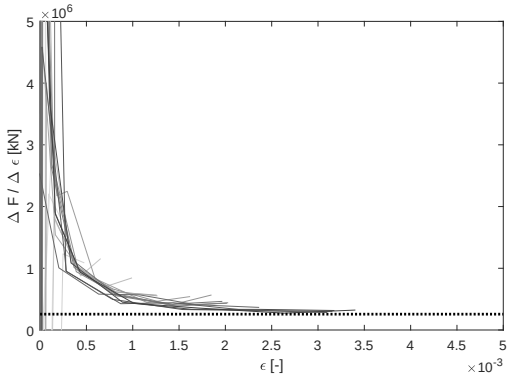

(c) Zone 4 - Depths from 8 m (light grey) to 11.2 m (dark grey).

Fig. 5. Application of Fellenius' method to determine the axial force in zones (a) 1, (b) 2, and (c) 4. For each load step, the ratio $\Delta F/\Delta\epsilon$ between the applied force increment ΔF and the measured strain increment $\Delta\epsilon$ is plotted against the measured strain. The asymptotic value for the tangential stiffness of the grout (dashed line, $(EA)_{\text{grout}} = 270000\,\text{kN}$) and the tendons stiffness (dotted line, $(EA)_{\text{strands}} = 256500\,\text{kN}$) is also indicated.

the grout-soil interface has been mobilized. In addition, the modulus of soil reaction k_s is estimated as the slope of the linear regression from figure 6 as 287.5 kN/m^2 for zone 1, 23606 kN/m^2 for zone 2, and 860.1 kN/m^2 for zone 4. These results indicate that the modulus of soil reaction is very high in the influence zone (zone 2), which is attributed to a distorted stress field and stress concentrations in the soil around the top of the tendon bond length, resulting from the sudden introduction of the anchor force in the grout volume at that particular location. In addition, it should be noted that the curves in figure 6 show no pronounced limit value, indicating that the soil has not fully been mobilized. As zone 4 has been subjected to post-grouting during the installation of the anchor, the resulting soil stiffness is larger than in zone 1, that has not been post-grouted.

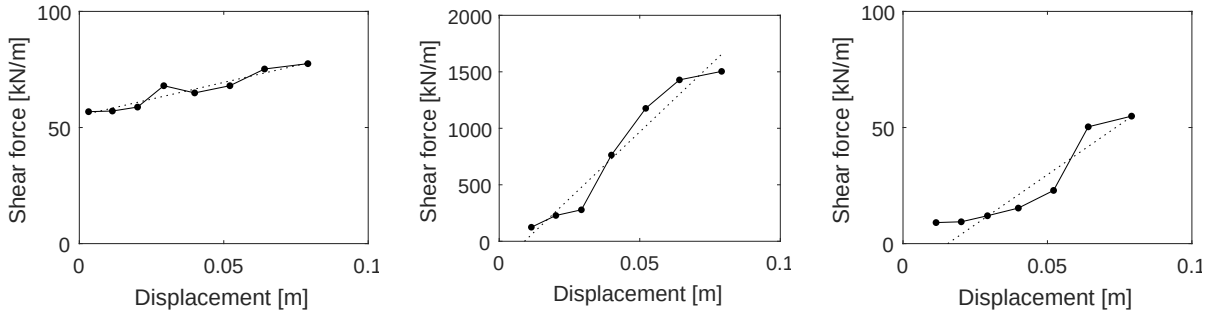

(a) Zone 1. **(b)** Zone 2. **(c)** Zone 4.

Fig. 6. Shear force $q(z)$ as a function of the anchor head displacement for zones (a) 1, (b) 2, and (c) 4 (solid line). The linear regression for the estimate of the modulus of soil reaction is also indicated (dashed line). Note that the vertical axis of the second figure is plotted on a different scale.

ANCHOR EXCAVATION

After the load test, the test anchor has been excavated as a part of the ground works on the construction site. The excavation has been gradually performed in stages of 2 m: at each stage, the grout body has been carefully unearthed and inspected, documenting the excavation by taking a number of photographs (figure 7). Before proceeding to a next excavation stage, the free standing grout column has been cut above ground level. The visual inspection of the grout body revealed longitudinal cracks in the grout body, in particular in the influence zone 2 and the transition zone 3, indicating a high degree of disintegration of the grout body. Furthermore, bulges in the tendon bond length are observed in zone 4, attributed to high-pressure grout flow along the soil-grout interface during post-grouting.

On the basis of the extensive set of photographs of the grout body, a three-dimensional (3D) photogrammetric model has been made (figure 7), resulting in an estimate of the average diameter and perimeter of the grout column as a function of depth. In the free length, the average diameter equals 0.187 m and the average perimeter equals 0.587 m. In the tendon bond length, the average diameter equals 0.189 m and the average perimeter equals 0.594 m. These result show that the diameter and perimeter of the grout body are not very different in the tendon free length and in the (post-grouted) tendon bond length. This is attributed to the relatively high soil strength and low soil compressibility for the site under consideration, resulting in a very limited cement grout penetration during post-grouting. From the estimate of the average grout diameter, the average

cross-section of the grout is found by subtracting the cross section of the steel strands from the total cross section of the grout column. In the free length and the tendon bond length this results in areas of 0.024 m^2 and 0.027 m^2, respectively.

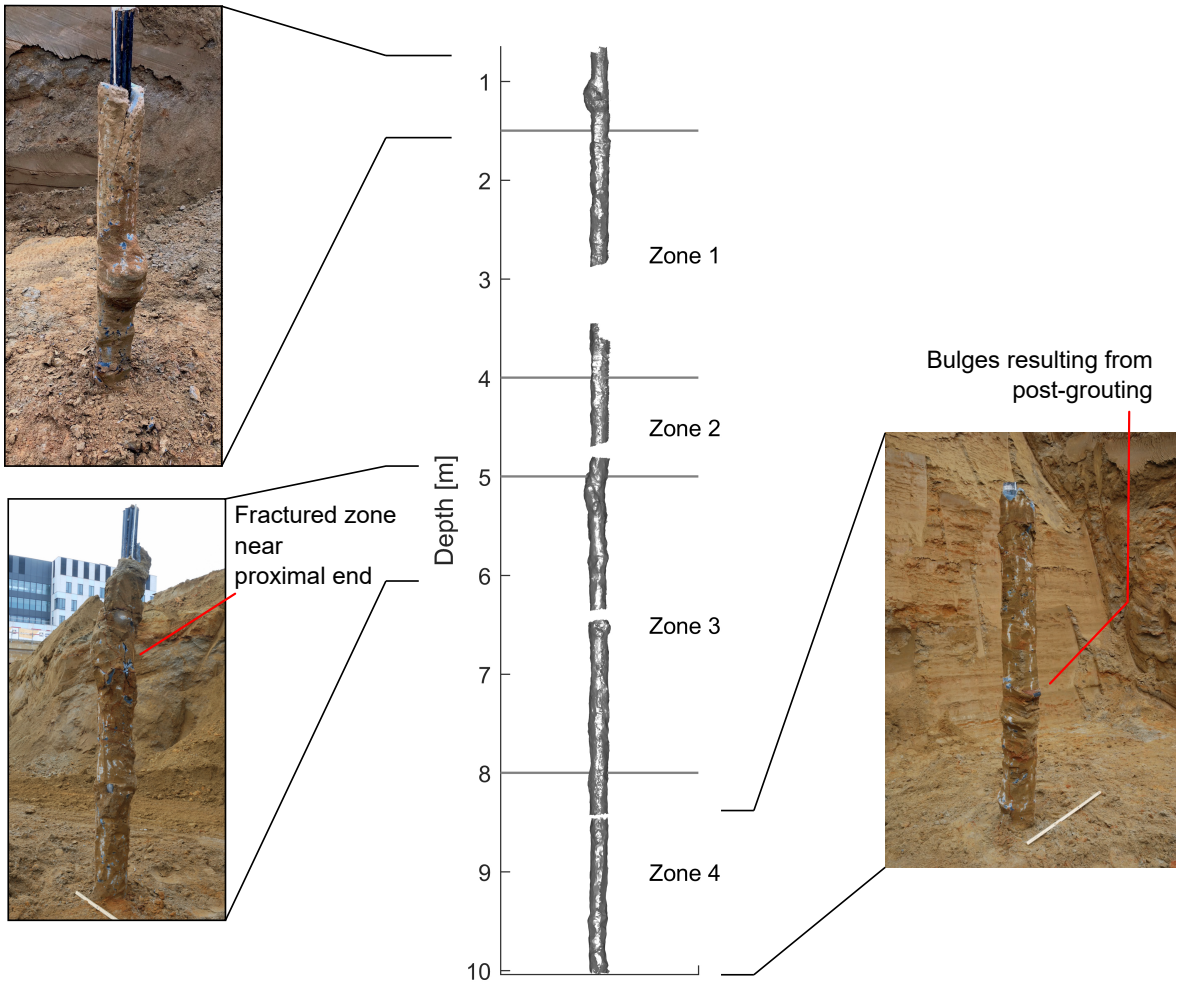

Fig. 7. 3D photogrammetric model of the grout body. The corresponding photographs indicate particular features along the anchor length.

NUMERICAL MODELING

In order to further interpret the results of the load test, a FE model is set up. A first option is the use of an axisymmetric or 3D FE model (Briaud and Lim 1999; Desai et al. 1986), where Coulomb friction theory relates the radial soil pressure and interface friction to the resulting interface strength. However, this approach does not account for a number of influence factors such as the drilling procedure, the grouting and post-grouting process, and penetration of cement grout in granular soil (Domes and Benz 2015). Since these factors have a large influence on the resulting anchor pull-out capacity, FE models require a lot of calibration of soil and soil-grout interface properties in order to obtain meaningful results. Therefore, an alternative approach is used in this paper. A 1D FE model is employed to provide a back-analysis of the experimental setup. The model parameters are calibrated in order to obtain a good correspondence and guide the interpretation of the strain measurements, allowing to reduce the uncertainty that is inherent to both measurements and numerical modeling of geotechnical structures (Gioda and Sakurai 1987).

In the FE model, the steel and the grout are separately meshed with 240 1D spring elements (figure 8). The interaction with the surrounding soil is modeled by means of elastic springs that account for the modulus of subgrade reaction. A vertical force is applied at the origin of the coordinate system, on the top node the steel strands. The nodes of the steel strand elements and the grout body elements are not connected in the tendon free length. In the tendon bond length, from a depth of 5 m, the connection between grout and steel is modeled by means of interface elements, that allow to model a progressive delamination between the grout body and the steel strands.

A linear elastic behavior is assumed for the steel strands, considering a Young's modulus of 190 GPa and a cross-section of $9 \times 150\,\text{mm}^2 = 1350\,\text{mm}^2$. Furthermore, the behavior of grout in compression is considered to be linear elastic. When the grout is subjected to tensile strains, the grout column will develop cracks, significantly reducing the overall grout stiffness. In order to account for the fracturing of the grout column in a simplified way, the assumption is made that the grout body has no stiffness in tension, whereas the stiffness in compression is estimated as $E_\text{g} = 5 \times 10^6$ kPa. The behavior of this no-tension material is modeled by considering a non-linear elastic model, for which the stress-strain response is shown on figure 8a. Hence, tensile strains in the grout do not induce stresses, in correspondence with opening cracks in the grout. Under compressive strains, the cracks close, which results in compressive stresses.

The measured shear force in figure 6 indicates that the soil strength has not been fully mobilized. Therefore, the interaction with the ground is modeled by means of linear elastic springs (figure 8b), representing the modulus of subgrade reaction of the soil. The spring stiffness in the free length, influence zone, and tendon bond length has been tuned in order to achieve a good correspondence between numerical results and measurements. This results in a stiffness of $6300\,\text{kN/m}^2$, $36000\,\text{kN/m}^2$ and $15000\,\text{kN/m}^2$ in the free length, influence zone, and tendon bond length, respectively. This stiffness is much larger than the stiffness estimated from the slope of the shear force in figure 6. This is due to the fact that the anchor head displacement is larger than the displacements of the grout body along the height, as a consequence of the delamination of the grout.

Interface elements are used to model the connection between grout and steel in the tendon bond length, accounting for the limited interface strength by means of a damage model (Phan et al. 2015; Spada et al. 2011). The damage model introduces a damage parameter ω following a classical damage mechanics framework (De Borst et al. 2012). The damage parameter $0 \leq \omega \leq 1$, is zero for an undamaged interface, 1 for a fully damaged interface, and can only increase. The damage parameter reduces the stiffness of the interface as $(1 - \omega)k$, following the relationship

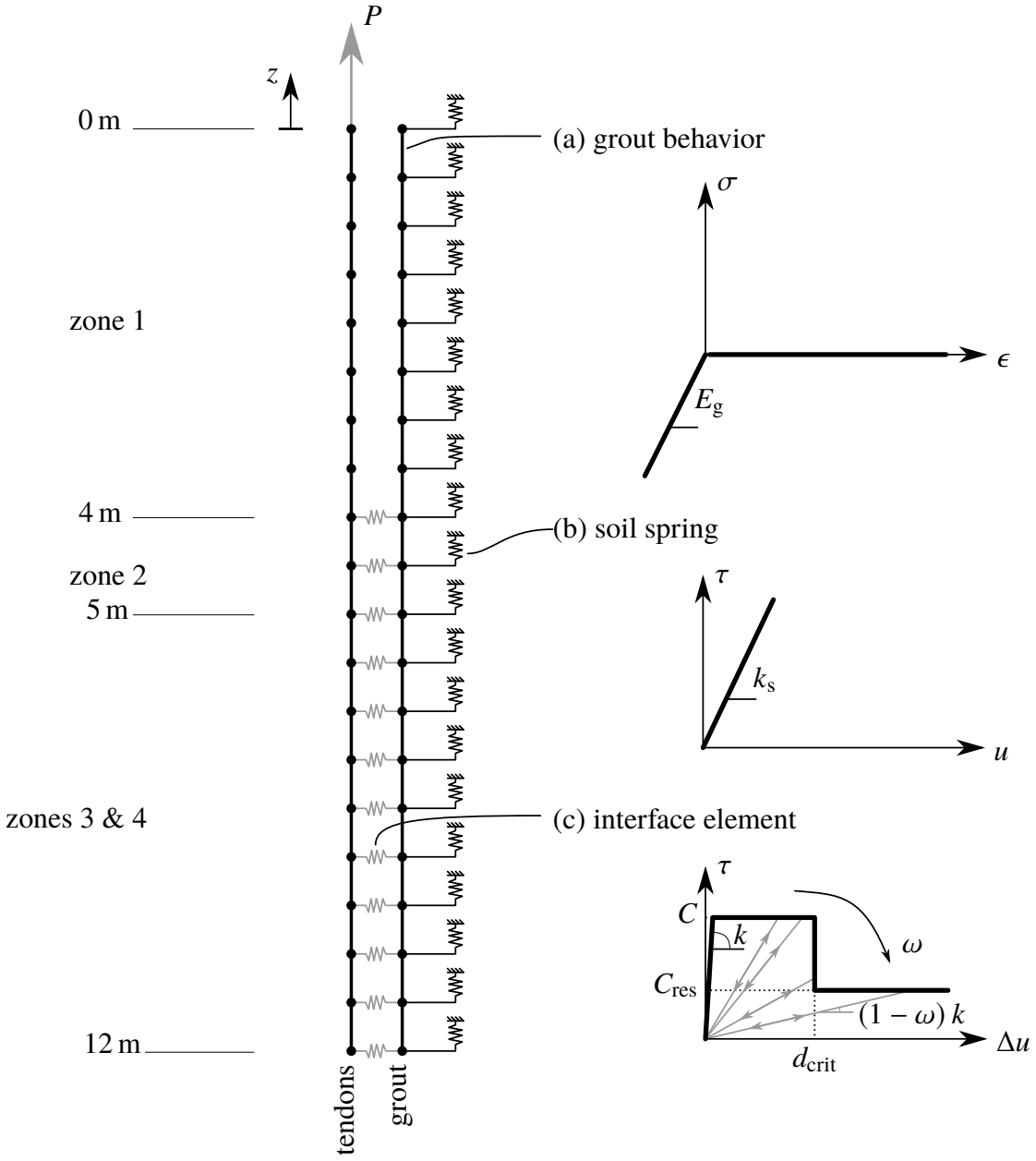

Fig. 8. Outline of the 1D finite element model with the stress-strain response of the (a) nonlinear elastic grout model, (b) elastic soil springs, and the (c) the interface element damage model where the loading-unloading curves are indicated in gray.

between interface shear stresses τ and the relative interface displacement Δu as shown in figure 8c. An initially very stiff connection between grout and steel is assumed, where a (dummy) stiffness $k = 10^9\,\mathrm{kN/m}$ is chosen so that the displacements between the grout and the tendons remain negligibly small for undamaged interface elements. The damage parameter starts to grow when a critical interface traction $\tau = C$ is reached (figure 8c), and this traction is maintained until the relative displacement between grout and steel reaches a limit value $\Delta u = d_{\mathrm{crit}}$. Next, the interface traction drops to a residual value $\tau = C_{\mathrm{res}}$, accounting for the presence of Coulomb friction between the tendons and the grout when delamination has fully developed (Phan et al. 2015; Spada et al. 2011). The parameters of the interface element have been obtained by parameter tuning in order to achieve a good correspondence between the observed and computed size of the delaminated zone (zone 3) at various load levels, resulting in $d_{\mathrm{crit}} = 10{\times}10^{-3}$ m, $C = 500\,\mathrm{kN/m}$ and $C_{\mathrm{res}} = 300\,\mathrm{kN/m}$.

The resulting non-linear finite element system of equations is solved using a global Newton-Raphson iterative scheme with a relative convergence tolerance of 10^{-6} on the residual forces in the equilibrium. Convergence with respect to mesh size has been checked, where the 240 elements over the height of the model is found sufficient to accurately capture the variations of the displacements and stresses over the anchor height.

The model is subjected to a load of 2000 kN, equal to the maximum test load from the in situ load test. The axial strains in the grout are shown in figure 9a and compared to the measured strains. There is a good correspondence between the model and the measurements in the tensile region (zone 4) and the influence zone just above the tendon bond length (zone 2). The transition zone 3 at depths between 5 m and 8 m shows different slopes for the tensile and compressive strains as a result of the no-tension stiffness of the grout. The 1D FE model is able to reproduce the behavior of the grouted anchor: the use of an interface damage model between grout and steel allows to explain the complex behavior of the grout body in the influence zone 3 as experimentally observed.

The axial strains and the axial force in the steel strands are plotted in figures 9b and figure 10a, respectively. The force in the strands remains equal to the applied force above the proximal end of the tendon bond length, where it starts decreasing due to the presence of shear forces between grout and steel. Due to the progressive delamination, the slope of the axial force curve (i.e. the rate of decrease of the axial force) is not constant. The delamination zone stretches deeper after every increase of the applied load. For a load of 2000 kN, the delamination occurs up to a depth of 8 m. The rate of decrease of the axial force is larger in the transition zone, where delamination has occurred, than in the intact tendon bond length. This is due to the fact that the broken grout is being pushed upwards, resulting in a transmission of shear forces between grout and soil in the influence zone just above the tendon bond length. It should be noted that the model predicts that only about 1000 kN of the applied force of 2000 kN is being transferred in zone 4.

The shear force between the anchor strands and the grout body is plotted in figure 10b, and should be interpreted together with the displacement jump between the grout body and the steel strands (figure 9c). Both figures show how the delamination progresses as the load increases. Initially, there is a rigid connection between grout and steel, and both the shear force and the differential displacement remain limited. At the onset of delamination, the relative displacement between the steel strands and the grout body increases and the shear force surges to its critical value, $C = 500\,\mathrm{kN/m}$. When the critical relative displacement $d_{\mathrm{crit}} = 10 \times 10^{-3}$ m is exceeded, the shear force drops to the residual value $C_{\mathrm{res}} = 300\,\mathrm{kN/m}$. The delamination further progresses as the load is increased, further mobilizing lower parts of the anchor. Figure 11 compares the modeled results of the anchor head as a function of the axial force during the load test with the

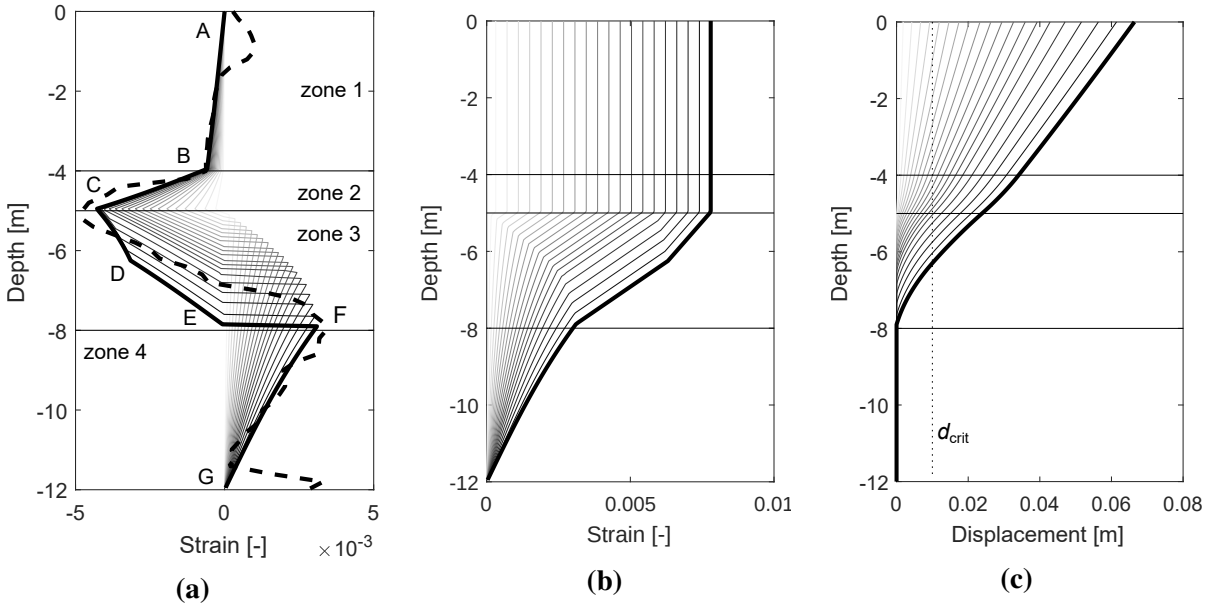

Fig. 9. Axial strains in (a) the grout body and (b) the steel strands, and (c) corresponding displacement between steel and grout for a load of 100 kN (light gray) to 2000 kN (black line). The measured strains in the grout at 2000 kN are also indicated (dashed line).

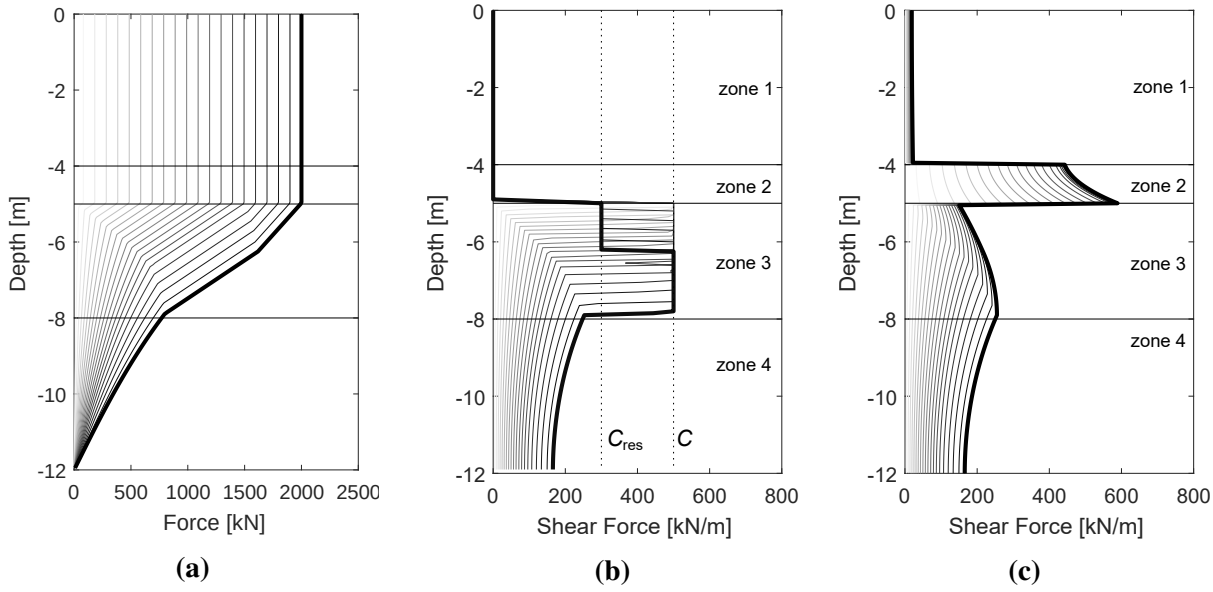

Fig. 10. (a) Axial force in the steel strands, (b) shear force between the steel strands and the grout, and (c) the shear force transferred between the grout and the soil. Results are shown for a load of 100 kN (light gray line) to 2000 kN (black line).

experimental values. The non-linearity of the curve is entirely attributed to the interface behavior and the no-tension stiffness of the grout. When the load on the numerical model is increased, the

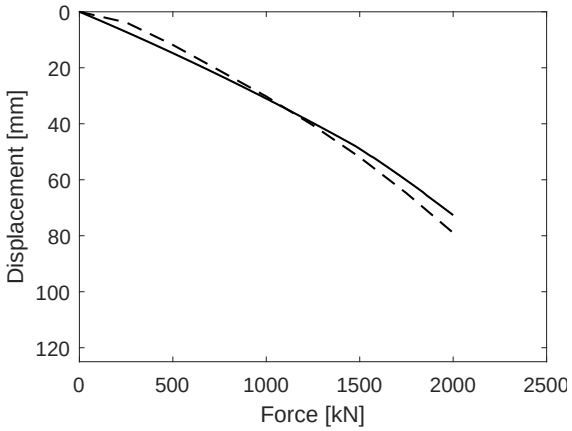

Fig. 11. Displacement of the anchor head as a function of the axial force during the load test. The result from the 1D model (solid line) are compared to the experimental values (dashed line).

ultimate limit load is reached at 2300 kN, corresponding to the the complete delamination of the interface. This demonstrates that the interface delamination might be an important anchor design aspect in the case where a high soil strength and stiffness is encountered.

Figure 10c shows the resulting shear force transmitted between the grout body and the soil through the soil springs. It is observed that, due to the high stiffness in the influence zone 2, a significant part (±20%) of the load is transferred from the anchor to the soil in this limited part of the tendon free length. A similar force transfer in the influence zone has also been observed in a test campaign at a site in Limelette, Belgium (Huybrechts et al. 2008).

CONCLUSION

In this paper, the behavior of a grouted anchor that has been installed on a construction site at the Health Sciences campus of KU Leuven has been studied. After the installation of the anchor using successive grout injections, it has been subjected to a load test up to the estimated anchor pull-out capacity. In order to gain detailed insight in the mechanical behavior, a robust and cost-effective procedure has been developed in order to measure the strains in the grout body using optical fibers. From these strain measurements it has been concluded that a delamination occurs in the tendon bond length between the steel tendons and the grout body. The upper delaminated part of the grout body is under compression whereas the lower bonded part of the grout body is under tension. This delamination gradually progresses as the anchor load increases.

The anchor behavior has also been modeled with a one-dimensional finite element model. The model includes the steel tendons and the grout body where an interface damage model is used to account for possible delamination of the interface. The soil has been modeled as a series of nonlinear springs for which the soil stiffness has been calibrated using the results of the load test. The results confirm that the observed compressive and tension zones of the grout body can be related to the interface delamination. Furthermore, a significant part of the load is transferred from the anchor to the soil the influence zone 2 at the proximal end of the tendon bond length.

The experiment and numerical modeling demonstrate how optical fiber measurements in the grout body can be used for the assessment of the anchor behavior, the mobilization of the soil resistance, and the estimation of the remaining anchor capacity. Consequently, the proposed measurement technique provides a valuable tool to perform long term health monitoring of grouted anchors under operational conditions.

REFERENCES

Barrias, A., Casas, J., and Villalba, S. (2016). "A review of distributed optical fiber sensors for civil engineering applications." *Sensors*, 16(5), 748.

Boyd, R. W. (2003). *Nonlinear optics*. Elsevier.

Briaud, J.-L. and Lim, Y. (1999). "Tieback walls in sand: numerical simulation and design implications." *Journal of geotechnical and geoenvironmental engineering*, 125(2), 101–110.

Bureau for Standardisation (NBN) (2013). "NBN EN 1537 - Execution of special geotechnical works - Ground anchors." *NBN EN 1537*, NBN.

Bureau for Standardisation (NBN) (2014). "NBN EN 1997-1/A1 - eurocode 7: Geotechnical design - part 1: General rules." *NBN EN 1997-1/A1*, NBN.

De Borst, R., Crisfield, M. A., Remmers, J. J., and Verhoosel, C. V. (2012). *Nonlinear finite element analysis of solids and structures*. John Wiley & Sons.

Desai, C., Muqtadir, A., and Scheele, F. (1986). "Interaction analysis of anchor-soil systems." *Journal of geotechnical engineering*, 112(5), 537–553.

Domes, X. and Benz, T. (2015). "Untersuchungen zur zementfiltration während der herstellung von verpressankern in nichtbindigen böden." *Bautechnik*, 92(9), 605–616.

Fellenius, B. H. (2001). "From Strain Measurements to Load in an Instrumented Pile." *Geotechnical News Magazine*, 19(1), 35–38.

Gächter, D., Kulmer, R., and Račanský, V. (2018). "Slope stabilization with multiple anchors monitored by glass fibre technique." *Proceeding of the 2018 DFI-EFFC International Conference on Deep Foundations and Ground Improvement, Rome, Italy*, Deep Foundation Institute, 494–503.

Gioda, G. and Sakurai, S. (1987). "Back analysis procedures for the interpretation of field measurements in geomechanics." *International Journal for Numerical and Analytical Methods in Geomechanics*, 11(6), 555–583.

Hong, C.-Y., Zhang, Y.-F., Li, G.-W., Zhang, M.-X., and Liu, Z.-X. (2017). "Recent progress of using Brillouin distributed fiber optic sensors for geotechnical health monitoring." *Sensors and Actuators A: Physical*, 258, 131–145.

Huang, M., Zhou, Z., Huang, Y., and Ou, J. (2013). "A distributed self-sensing frp anchor rod with built-in optical fiber sensor." *Measurement*, 46(4), 1363–1370.

Huybrechts, N., De Vos, M., Tomboy, O., and Maertens, J. (2008). "Integrated analysis of the load test results & suggestions for a harmonised anchor design and test methodology in Belgium in the Eurocode 7 framework." *Proceedings of the International Symposium "Ground Anchors Limelette Test Field Results", 14 May 2008, Brussels*, Scientific and Technical Centre for Building, <available from: https://www.cstc.be>.

Huybrechts, N., De Vos, M., and Van Lysebetten, G. (2016). "Advances and innovations in measurement techniques and quality control tools." *International Symposium on Design of Piles in Europe*.

Huybrechts, N., Van Lysebetten, G., and De Vos, M. (2017). "Advanced monitoring techniques for a wide range of geotechnical applications." *ICSMGE 2017 - 19th International Conference on Soil Mechanics and Geotechnical Engineering*, 2761–2764.

International Organization for Standardization (2018). "ENISO22477-5 - Geotechnical investigation and testing - Testing of geotechnical strucures - Part 5: Testing of anchorages." *ENISO22477-5*, ISO.

Mecsi, J. (1997). "Some practical and theoretical aspects of grouted soil anchors." *Ground anchorages and anchored structures: Proceedings of the international conference organized by the Institution of Civil Engineers and held in London, UK, on 20–21 March 1997*, Thomas Telford Publishing, 119–130.

Phan, T. S., Rossi, P., and Tailhan, J.-L. (2015). "Numerical modelling of the concrete/rebar bond." *Cement and Concrete Composites*, 59, 1–9.

Spada, A., Giambanco, G., and Rizzo, P. (2011). "Elastoplastic damaging model for adhesive anchor systems. I: theoretical formulation and numerical implementation." *Journal of engineering mechanics*, 137(12), 854–861.

Štefaňák, J., Miča, L., Chalmovskỳ, J., Leiter, A., and Tichỳ, P. (2017). "Full-scale testing of ground anchors in neogene clay." *Procedia Engineering*, 172, 1129–1136.

Yu, H. and Houlsby, G. (1991). "Finite cavity expansion in dilatant soils: loading analysis." *Géotechnique*, 41(2), 173–183.

Zeni, L., Picarelli, L., Avolio, B., Coscetta, A., Papa, R., Zeni, G., Di Maio, C., Vassallo, R., and Minardo, A. (2015). "Brillouin optical time-domain analysis for geotechnical monitoring." *Journal of Rock Mechanics and Geotechnical Engineering*, 7(4), 458–462.